Journal of Water Process Engineering 7 (2015) 187–195

Contents lists available at ScienceDirect

Journal of Water Process Engineering

journal homepage: www.elsevier.com/locate/jwpe

UV–visible light-activated Au@ pre-sulphated, monodisperse TiO_2 aggregates for treatment of congo red and phthalylsulfathiazole

Dongfang Zhang*, Jiaxun Wang

[a] College of Science, Huazhong Agricultural University, Wuhan 430070, PR China

ARTICLE INFO

Article history:
Received 1 April 2015
Received in revised form 24 June 2015
Accepted 28 June 2015

Keywords:
Photocatalysis
Dye abatement
Gold deposition

ABSTRACT

Liquid-phase photocatalytic oxidation of a secondary diazo dye compound, Congo red (CR, $C_{32}H_{22}N_6Na_2O_6S_2$) and pharmaceutical phthalylsulfathiazole, was carried out in a cylindrical photochemical reactor on gold-loaded titania systems. The deposition of Au nanoparticles was performed by photochemical deposition methods on the surface of pre-sulphated titania. The detailed structural, compositional and optical characterization and physico-chemical properties of the obtained products are analyzed by X-ray diffraction (XRD), energy dispersive X-ray (EDX), transmission electron microscopy (TEM), high resolution TEM (HRTEM), UV–vis diffuse reflectance spectroscopy (UV–vis DRS), Fourier transformation infrared spectroscopy (FTIR) and photoluminescence spectra (PL) analysis. Notable enhancements in the photocatalytic activity of TiO_2 were achieved by deposition of gold onto titania, which can be attributed to the enhanced surface electron excitation and effective electron-hole separation on gold-deposited TiO_2 nanoparticles. The present study shows that the higher rate of photodegradation observed on Au-TiO_2 at pH 6.5 can be correlated to the ratios of the concentrations of the ionized to the neutral dye molecules and also to the higher concentration of hydroxylated surface, which are able to effectively scavenge photogenerated valence band holes. Accumulation of the holes in the semiconductor particles increases the probability of formation of excited oxygen atom which is a reactive species readily oxidizing the organic dye molecule or environmental pollutant such as pharmaceutical phthalylsulfathiazole. The reaction mechanism of the photocatalytic system was detected by a photoluminescence method using terephthalic acid as a probe molecule.

1. Introduction

Nowadays, dyes are widely used in industries such as textile, rubber, paper, plastic, cosmetic etc. Wastewater from dyeing processes contains a wide variety of water soluble chemical products that are unsuitable to treat by traditional methods like filtration, carbon absorption and hypochlorite oxidation. Most of the dyes used in textile industry are highly stable, soluble in water, resistant to chemical oxidation and will have low bio-degradability. Dyes can be divided into several categories, based on their chemical nature: anionic or cationic and basic or reactive dyes. Azo dyes are the largest group of the synthetic colorants known and the most common group released into the environment. Wastewater containing dyes may be toxic, carcinogenic and mutagenic [1]. Therefore, the removal of synthetic dyes with azo aromatic groups is extremely important. The development of new technologies for wastewater purification tends to reach complete destruction of the contaminants. Recently, advanced oxidation processes (AOPs) have been proposed as alternative methods for water purification, which is based on in situ generation of hydroxyl radicals, a strong oxidizing agent and can oxidize almost all the organic pollutants and mineralize them to CO_2, H_2O and simple mineral acids. AOPs include photocatalysis systems such as combination of a semiconductor (TiO_2, ZnO, etc.) and UV light. TiO_2 is the widely used photocatalytic materials in various fields. TiO_2 has been widely used because of its various merits such as low cost, superior chemical resistance, nontoxicity and high efficiency for mediating difficult-to-remove pollutants [2]. Specially, TiO_2 nanoparticles could serve as an excellent source for the photocatalytic decomposition of organic pollutants in water. It is anticipated that, in the presence of TiO_2 nanoparticles, sewage water could be gradually purified under the influence of sunlight. Photocatalytic activity of TiO_2 depends on the rate of generation of free radicals (electrons and holes), which are formed when semiconductor is excited with the wavelength energy equals or higher than the energy of its band gap (UV or visible light), their reactivity and their recombination rate. The

* Corresponding author.
E-mail address: jiaxun123wang@yeah.net (D. Zhang).

http://dx.doi.org/10.1016/j.jwpe.2015.06.013
2214-7144/

mechanism of the destruction of organic compounds can go indirectly owing to the attack of OH radicals, which are formed after the reaction of photogenerated holes with adsorbed water on the surface of the semiconductor or directly by the reaction of adsorbed organic molecules on the surface of semiconductor with holes or active centers (surface defects) [3–6].

Currently, however, the highly efficient use of TiO_2 in photocatalytic application has been limited by several reasons such as low photon utilization efficiency and need for a high power UV excitation source. Following excitation of materials such as crystalline TiO_2, recombination of e^-/h^+ pairs is the most thermodynamically favored pathway in the absence of molecules used to scavenge either photogenerated electrons or holes. It has been estimated that <5% of charges in these systems can actually be utilized to induce redox reactions at the interface [7]. This is a problem inherent to all large-band-gap metal oxides currently being explored as UV active photocatalysts. Incorporation of noble metal nanoparticles of Au, Ag, and Pt into semiconducting metal oxides has been shown to enhance photocatalytic activity [8,9]. Especially, the addition of gold nanoparticles has been used to enhance the photoactivity of TiO_2, and the development of this strategy remains an important area of investigation within photocatalysis. Nanoparticles of gold and other noble metals deposited on the TiO_2 surface have been reported to increase the efficiency of the photocatalytic process by acting as electron sinks, facilitating electron-hole separation, promoting the interfacial electron transfer process and decreasing the recombination rate of photogenerated charges [10,11]. It is proposed that the noble metals mediate the photocatalytic process by storing and shuttling photogenerated electrons from the semiconductor to an acceptor [12]. Besides, a synergetic increase in the photocatalytic activity of metallized TiO_2 which had been previously sulfated has been reported [13]. It was found that sulphation shields the TiO_2 surface area against sintering, stabilizing the anatase crystalline form at high calcination temperatures and producing at the same time a highly defective surface. This results from the creation of oxygen vacancies via a dehydroxylation process during calcination. In regard to this, nonstoichiometry has been reported to influence the adsorption energy of noble metals on TiO_2, also altering significantly the electronic structure of the metal adlayers. Thus, oxygen vacancies have been proved to be preferential sites for metal adsorption. This leads to a better charge-transfer between metal and semiconductor with a consequent increase in the effectiveness of charge separation and therefore in the efficiency of photocatalysis [14]. In this regard, the present work reports the synthesis of highly active gold metallized pre-sulphated TiO_2 nanocomposite photocatalyst using a simple photochemical reduction method by embedding gold nanoparticles, a highly stable inorganic photosensitizer, homogenously within TiO_2 matrix. The effects of Au nanoparticles on the microstructures and photocatalytic behaviors of the as-prepared Au-TiO_2 nanocomposite catalyst, which is compared with the commercial titanium dioxide from Aladdin for the photocatalytic removal of aqueous Congo Red (CR) solution were investigated and discussed in detail.

2. Experimental

Titanium dioxide (TiO_2) catalyst (M_w = 79.87, hydrophilic) purchased from Aladdin Chemistry Co. Ltd, with purity 99.8%, was used as received, without further modification. It is mostly in the anatase form, nonporous, with a reactive surface (BET) area of about 52.0 m^2/g and a mean particle size of around 25 nm. Congo Red (CR, $C_{32}H_{22}N_6Na_2O_6S_2$) was supplied by ACROS, as high purity biological stain, and used as a model compound without further purification. Phthalylsulfathiazole (98%) were supplied by Tokyo Kasei Kogyo Corporation (Tokyo, Japan), and the stock solutions for phthalylsulfathiazole compounds (200 mgL^{-1}) were prepared by dissolving suitable amount solid reagents with deionized water. All solutions were prepared using double distilled deionized water. The preparation of gold metallized pre-sulphated titania (Au–TiO_2-s) catalyst was as follows. At first, sulphated TiO_2 (TiO_2-s) was prepared by immersing the precipitate in 1 mol/L sulphuric acid solution for 2.0 h. The precipitate was then filtered again, dried at 120 °C overnight and calcined at 600 °C for 2.0 h. The calcination temperature selected for both materials is reasonable to produce samples with optimum photocatalytic activity in the degradation of dye molecule since commercial TiO_2 should not be calcined at 700 °C as this temperature leads to a nearly complete loss of the surface area and total rutilisation of the material, and consequently to a very poor photocatalytic activity. Nonetheless, pre-sulphated TiO_2 should not be calcined at 500 °C as this temperature is not high enough to eliminate sulphate groups from the TiO_2 surface, leading equally to a poor photocatalytic activity either. Noble metal modification of the calcined TiO_2 samples was performed by photodeposition route. Gold doping was achieved using tetrachloroauric acid ($AuCl_3{\cdot}HCl{\cdot}4H_2O$), Sigma–Aldrich, 99.9%) as precursors. Solutions of the appropriate concentrations of metal chloride (corresponding to a 1.0 wt% metal loading) in distilled water were prepared and mixed with suspensions of the TiO_2 in distilled water (10 g TiO_2 L^{-1}), adding 0.50 mol/L absolute ethanol as sacrificial donor. Photodeposition was performed by illuminating the suspensions for 5.0 h with a 300 W high-pressure mercury lamp of photon flux ca. 3.0×10^{-7} Einstein s^{-1} L^{-1} in the $\lambda < 400$ nm region while maintaining continuous nitrogen purging under vigorous stirring. After irradiation, the derived sample was washed twice with water, centrifuged and dried at 100 °C overnight. Hereafter the as-prepared sample will be denoted by Au–TiO_2-s (sulfated and Au metallised) followed by the nominal metal content 1.0 wt% gold loading on the surface of titania. For comparison, the commercial TiO_2 nanopowders (made from Aladdin Chemistry Co. Ltd) without sulphication treatment and gold modification were used in this study as the reference sample (denoted as b-TiO_2) since use of colloidal photocatalyst may not be attractive in an online system of photodegradation process.

X-ray powder diffraction (XRD) data were recorded at room temperature with an X-ray diffractometer (XRD-6000, Shimadzu Corporation) using Cu Kα irradiation (λ = 0.15408 nm), operated at 40 kV and 100 mA, which was used to identify the crystallographic information such as structure properties, chemical composition and phases of the products. The size and morphology of the samples were characterized by transmission electron microscopy. The observation and recording of TEM images were performed with a HITACHI H-7650 transmission electron microscope at 80 KV and a Gatan 832CCD camera. High-resolution transmission electron-microscopy (HRTEM) images were conducted on a JEOL JEM-2010 instrument operated at an accelerating voltage of 200 kV. The EDX analysis was done using Oxdord INCA 250 energy dispersive X-ray microanalyzer. The percentage of UV–vis reflectance was measured by diffuse reflectance spectroscopy (DRS) for the powder form of the catalysts using a scanning UV-vis-NIR spectrophotometer (Varian Cary 500) in the region of 200–800 nm. The spectrophotometer was equipped with an integrating sphere assembly and polytetrafluoroethylene was used as a reflectance material. The reflectance data were converted to the absorbance values, F(R), based on the Kubelka–Munk theory. The photoluminescence (PL) emission spectra of the samples were measured with a RF-5301 PC spectrofluorophotometer (Shimadzu Corporation) by using the 320 nm line of a Xe lamp as excitation source at room temperature. To detect the hydroxyl radicals (•OH) groups in as-prepared Au–TiO2/s catalyst, the following method was used: the sample was placed in a 50 ml aqueous solution of 1.0×10^{-4} mol L^{-1}

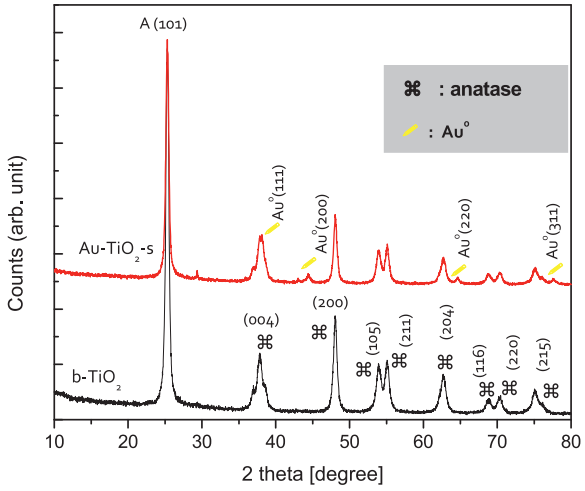

Fig. 1. X-ray diffraction patterns of the b-TiO_2 and 1.0 wt% Au–TiO_2-s samples (symbol ⌘ : anatase).

terephthalic acid and 4×10^{-4} mol L^{-1} NaOH in a beaker at ambient temperature, and subject to the illumination of UV–visible light source (provided by a 500 W xenon lamp) at the intervals of irradiation time (0, 10, 20, 30, 40, 50, 60 and 70 min). A 5 ml of the suspension was collected. PL spectra of the 2-hydroxy terephthalic acid produced by the reaction between terephthalic acid and photogenerated hydroxyl radicals were recorded on a Shimadzu RF-5301 PC spectrometer using Excitation wavelength of 315 nm, and scanning light wavelength of 350–600 nm.

Catalytic activity for both photocatalysts was measured in a liquid phase photocatalytic oxidation of Congo Red (CR), which was chosen as a model compound to evaluate the photoactivity of the as-prepared systems. The artificial light photocatalytic activity test is conducted in a quartz photoreactor with a cylindrical configuration. A 500 W Xenon lamp (the wavelength of the lamp is 300–780 nm) is positioned inside the reactor to simulate UV–visible light source. The distance between the surface of reaction solution and light source is adjusted to about 12 cm. A certain amount of photocatalyst powder (25 mg) is added to 200 ml aqueous Congo Red (20 mg/L). Before the occurrence of the photocatalytic degradation, the suspension is magnetically stirred in the dark for about 60 min to establish a Congo Red adsorption/desorption equilibrium. During the irradiation experiments, samples of 5 ml are withdrawn from the suspension at appropriate intervals and are immediately centrifuged at 8000 r/min for 20 min to remove solids. The concentration of Congo Red after illumination is monitored at λ = 498 nm using UV–vis spectrophotometer (Spectrumlab 22). The degradation rate (η) of the Congo Red can be determined by the formula: $\eta = (C_0\text{-}C)/C_0 = (A_{0max}\text{-}A_{max})/A_{0max}$, where C_0 and A_{0max} are the concentration after equilibrium adsorption and absorbance of Congo Red solution at 498 nm corresponding to maximum absorption wavelength after equilibrium adsorption of the dye; C and A_{max} are the concentration and absorbance of Congo Red solution at 464 nm after simulated solar light illumination.

2. Results and discussion

Crystalline phase composition of the samples was studied by XRD technique and XRD patterns for bare TiO_2 and pre-sulphated TiO_2 with 1.0 wt% photodeposited metal Au, are shown in Fig. 1. Five distinct diffraction peaks of both samples are indexed to anatase (JCPDF 21–1272) with high crystallinity, and the peaks at 25.3, 37.5, 48.0, 53.8, 54.9, and 62.5° 2θ were assigned to the (1 0 1), (0 0 4), (2 0 0), (1 0 5), (2 1 1), and (2 0 4) lattice plane reflections of tetragonal anatase, indicating the developed Au–TiO_2-s composite existed primarily as anatase. Moreover, no peaks corresponding to the rutile phase can be observed for the Au-modified TiO_2 photocatalyst. Since the crystal structure of TiO_2 is determined mainly by the heat treated temperature and it is well known that the transition from anatase to the rutile phase usually takes place when the calcination temperature is higher than 500 °C. It is proposed that pre-treatment with sulphuric acid clearly has the effect of stabilizing both the TiO_2 surface against sintering and inhibits conversion of the anatase crystal structure to the rutile form up to calcination temperatures as high as 600 °C. Therefore, there was little crystal transformation occurred in the sulfate pretreatment along with Au modifying procedures and the developed Au–TiO_2-s composite has anatase crystals when annealed at 873 K. Stabilization of the metastable anatase crystal structure is essential as it is known that it possesses higher photoactivity as compared to the thermodynamically stable rutile phase TiO_2 [15]. Clearly, the addition of noble metals did not alter the phase composition or the basic crystal structure of the TiO_2 (tetragonal, $a = 0.37845$ nm, $c = 0.95143$ nm, body centered). Neither the position nor the width of the peaks changed significantly after deposition, which indicates that there was no distortion of the original TiO_2 structure. At first glance, no metallic Au characteristic diffractions appear in XRD profiles. If metallic Au diffractions appear, a peak is expected at 38.2° for Au(^{0}). Nevertheless, metallic Ti (002) reflection peak ($2\theta = 38.4°$) would overlap this Au (1 1 1) reflection. However, slow scanning (0.5°/min) shows in the Au–TiO_2-s sample some weak peaks associated with the metal deposits were observable. In the Au–TiO_2-s material, two reflections at diffraction angles (2θ) of about 44.5° and 65° assignable respectively to diffraction on the (2 0 0) and (2 2 0) planes of metallic gold (Au^0) were recorded. It can be found that that the Au (2 0 0) diffraction peak ($2\theta = 44.5°$) is rather weak, which indicates that the deposited Au NPs may not be easily detected by XRD due to the low Au loading or ultra-fine size. Since no characteristic peaks corresponding to other dopant containing species are present, it can be concluded that the Au loading is below the dispersion capacity. Also, the 2θ values at which the major peaks appeared were found to be almost the same for both TiO_2 and Au–TiO_2 which indicated that the TiO_2 crystal structure was not altered while doping with Au nanoparticles. This means the Au nanoparticles are deposited in the surface of the TiO_2 nanoparticles and not inserted in the crystal lattice. By applying the Scherrer formula, the average crystalline size of TiO_2 sample is estimated to 23 nm according to the strong (1 0 1) anatase reflection peak ($2\theta = 25.1°$). Qualitative determination of Au–TiO_2-s sample was studied by EDX technique as shown in Fig. 2 by using grid supported carbon film of 15–25 nm thickness which gives exceptionally low background. The result indicates that C, O and Ti as the major elements with strong Au peaks in the composites. In addition, nano-TiO_2 shows a peak around 0.2 keV and another intense peak appears at 4.5 keV. The intense peak is assigned to the bulk TiO_2 and the less intense peak to the surface TiO_2 [16]. The peaks due to metallic Au are clearly distinct at 1.2, 2.5 and 8.5 keV, which confirm that Ti, O and Au exist in the catalyst structure and the deposition of Au on the surface of titania. The numerical results including the atom and weight percentage (atomic% and weight%) values of EDX quantitative microanalysis of the sample shows that the chemical composition of element of metallic Au is 0.123 at% or 0.90 wt% in the Au deposited TiO_2 composite, which is consistent with the theoretical nominal content of deposited gold. There were some small impurities, which were attributed to the use of commercial titania as the holder of Au without further purification. The presence of carbon signal arises from the TEM grid. Apart from that no other element peaks could be detected. On the whole, oxygen and titanium were present as major elements with small quantities of gold in the composite in the as-prepared compound. The as-prepared

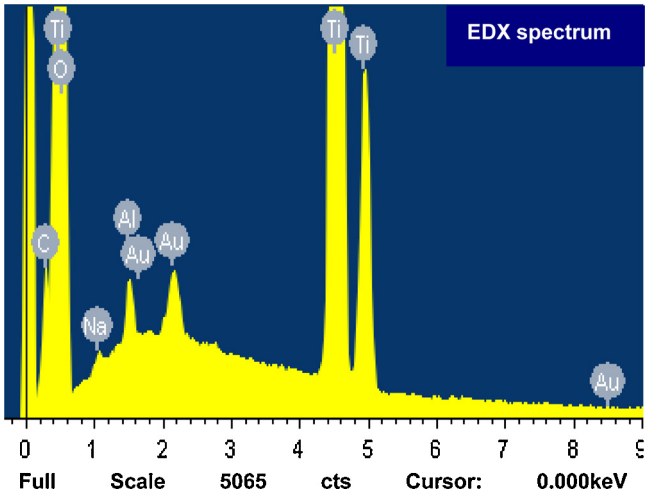

Fig. 2. EDX elemental microanalysis of 1.0 wt% Au–TiO_2-s nanoparticles.

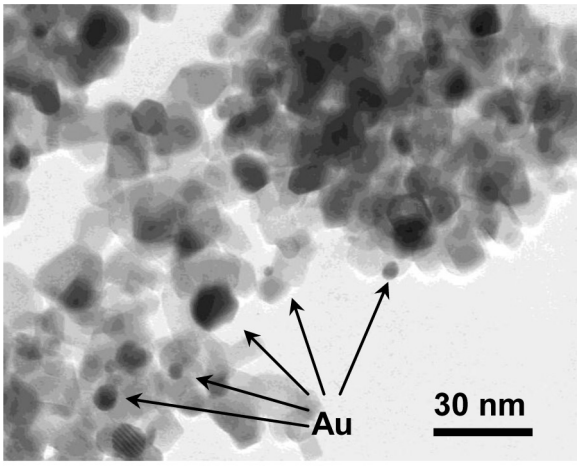

(a)

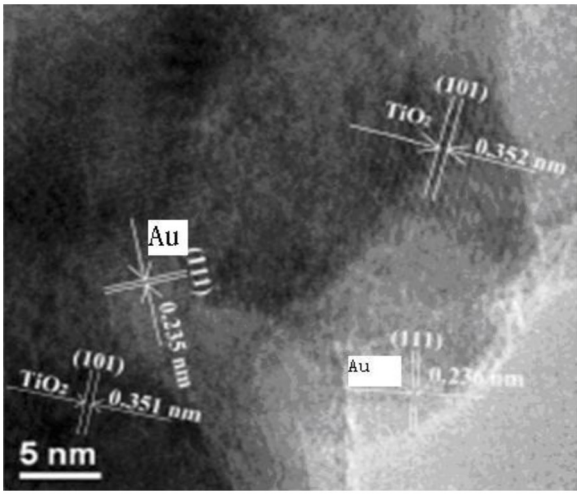

(b)

Fig. 3. Bright field TEM image (a) of HRTEM image (b) of 1.0 wt% Au–TiO_2-s sample prepared by photodeposition onto sulfated TiO_2.

Au–TiO_2-s sample was further characterized by TEM techniques to obtain some information about the particle sizes and surface morphology during modification, as is can be seen in Fig. 3. It could be seen that the primary TiO_2 particle sizes ranged from 20 to 30 nm,

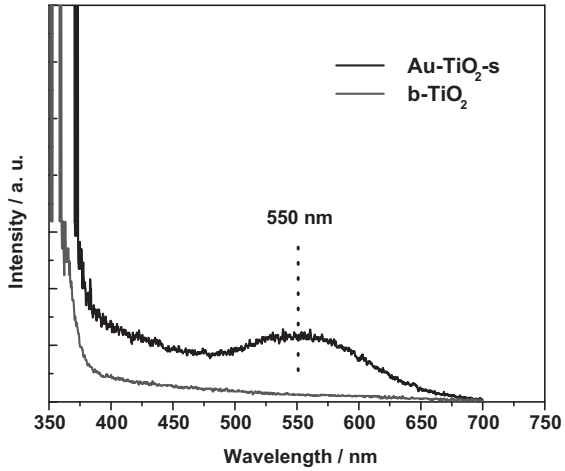

Fig. 4. UV–visible absorption spectra of b-TiO_2 and 1.0 wt% Au–TiO_2-s samples.

which were in good agreement with the value of the crystallite size determined by XRD spectra. Furthermore, it showed that Au metal particles were randomly dispersed on the TiO_2 surface (showed by the arrowhead). The TEM micrograph permits easy differentiation of Au nanocrystals (small dark areas or dark spots) and TiO_2 crystallites (large bright areas). At first glance, a large number of spherical metal nanoparticles or clusters dispersed on the surface of TiO_2 were clearly observed as the darker spots and these spherical particles are fairly stable, well defined and discrete. Metallic Au deposits were well distributed over many of the crystal surface of TiO_2 nanoparticles, even though this caused partial agglomeration to form block particles since the photodeposition method leads to heterocoagulation where the nanosized Au deposits are formed on the surface of TiO_2 crystallites. That is Au nanocrystals are seen on the surface of the TiO_2 particle as dark dots. Besides, there is a possibility of for the metallic Au to be inserted into the interstitial positions of the adjacent semiconductor particles. The corresponding HRTEM image clearly illustrated the twin boundaries due to the presence of gold nanoparticles (~3–5 nm size) on the TiO_2 matrix. The Au nanoparticles were supported on the TiO_2 surface with a condensed shape having a large interfacial area because of the low interfacial energy between gold nanoparticles and TiO_2 [17]. It was observed that the Au nanoparticles were highly dispersed on the TiO_2 surfaces. Meanwhile, the HRTEM image clearly displayed periodic fringe spaces of 0.351 nm and 0.235 nm indicative of highly crystal-lized anatase (1 0 1) TiO_2 planes and Au (1 1 1) planes, together with the formation of heterojunctions at the interface between Au and TiO_2.

Light absorption properties were studied by UV–vis spectroscopy and the absorbance spectra of the as-prepared samples are shown in Fig. 4. The strong plasmon resonance absorption at wavelengths above 400 nm is observed due to the Au nanoparaticle deposition on TiO_2. Light absorption by the deposited metal causes a collective oscillation of the free conduction band electrons of the gold nanoparticles as a consequence of their optical excitation. This phenomenon is observed when the wavelength of the incident light far exceeds the particle diameter. We propose a mechanism describing the deposition and growth of gold particles on the titania surface. Gold ions are initially adsorbed on the surface of TiO_2 particles. Photogenerated electrons reduce adsorbed Au^+ ions to gold metal atoms. The formation of small crystallites of gold can occur either by the agglomeration of gold atoms or by a cathodic-like successive reduction process. The agglomeration of gold atoms can be described in the following way: TiO_2 (e^-, h^+) + Au^+ adsorbed → TiO_2–Au^0(h^+). The successive reduction sequence is represented by: $mAu^0 \rightarrow Au_m$. In UV–vis diffuse

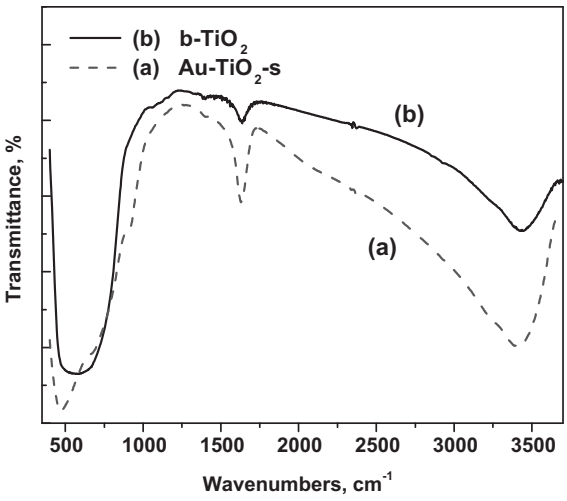

Fig. 5. FT-IR spectra of TiO_2 nanoparticles: (a) 1.0 wt% Au–TiO_2-s and (b) unmodified TiO_2.

reflectance spectroscopy, bare TiO_2 particles exhibit a single and broad intense absorption band at ~400 nm, which corresponds to the charge-transfer transition ($O^{2-} \rightarrow Ti^{4+}$) between the lattice oxygen ligands (O^{2-}) and a central titanium ion (Ti^{4+}) with octahedral coordination. This type of intrinsic band gap absorption associated with electronic excitation from the 2p level of oxygen (valence band) to 3d level of titanium (conduction band). The addition of metallic gold did not affect significantly the absorption edge of the TiO_2 in any case and it can be found that unmodified TiO_2 and Au–TiO_2-s composite catalyats have great absorption at the ultraviolet region. Nonetheless, in the visible part of the spectra the surface plasmon absorption corresponding to gold can be observed with maxima around 550 nm. When at the visible region, Au–TiO_2-s composite have good absorption, this also means the as-prepared composite has great photocatalytic activity under visible light irradiation. The absorption of visible light by metallised sample has been ascribed to low-energy transitions between the valence band of TiO_2 and localized energy levels introduced to the band-gap by deposited metal clusters [18]. As metallic Au can retard the charge-pair recombination and can trap electrons on the conduction band, Au–TiO_2 has good adsorption at the visible region. Because of the synergistic reaction of metallic Au and TiO_2, the adsorption effect of Au–TiO_2 is good at the visible region. Besides, it has been reported that the surface plasmon resonance of gold nanoparticles may assist in the separation of photogenerated charges created in the TiO_2 [19], which could contribute to the enhancement of photocatalytic activity of Au modified titania sample studied here, as it will be discussed later. As shown in Fig. 5, the infrared spectra of bare TiO_2 and Au–TiO_2-s powders in the range 400–4000 cm^{-1} shows a broad band at 3400 cm^{-1} which can be assigned to γ_{OH} stretching mode of O—H vibration of the Ti—OH. The other narrow band at 1632 cm^{-1} can be assigned either to δ_{OH} bending modes of hydroxyl group. These results strongly confirm the presence of hydroxyl ions in the structure of the samples. When the calcination temperature increased further, the intensities of the various bands related to hydroxyls were obviously decreased, indicating that the hydroxyl ions were gradually diminished (not shown here). However, even the sample calcinated at 600 °C has the bands corresponding to OH^-. These results show the structural network still retains some hydroxyls. There is no band centered at 1389 cm^{-1} that is assigned to bending vibrations of C—H bond in the species linking —Ti—O—Ti— structural network. In the region below 1000 cm^{-1}, several peaks were ascribed to absorption bands of Ti—O (550–650 cm^{-1}) and O—Ti—O flexion vibration (430–520 cm^{-1}). The FT-IR results are in good agreement with the XRD analysis and no alkoxy groups and sulphuric acid exist in the samples. Because the photochemical reactions primarily take place on catalyst surfaces, the chemical species adsorbed on surface could play an important role on the photocatalytic properties. By comparison, it can be found that the intensity of 1627 and 3400 cm^{-1} peak signal, which caused by the vibration absorption of free water and the hydroxyl function groups since water is adsorbed on TiO_2, both molecularly and dissociatively, increases for gold modified TiO_2 sample, indicating its surface to be more hydroxylated compared to neat TiO_2. Therefore, the FTIR investigation confirms that Au–TiO2 system contains more surface hydroxyl or larger surface OH group density than pure titania. The larger surface hydroxyl group density will lead to enhancement of the photocatalytic activity because photo-induced hole trapping by either the surface hydroxyl groups or the adsorbed water molecules generates short-lived $HO^{\bullet}$ radicals, which are the primary oxidizing agents in the photomineralization of organics [20–22], whereas a fraction of these electron-hole pairs reach the crystal surface and react with adsorbed substrates can suppress the high degree of recombination between the photogenerated electrons and holes as a major factor reducing photocatalytic efficiency [23]. The adsorbed oxygen molecule take up the electron to produce highly active superoxide radical ($O_2^{\bullet -}$). In the presence of moisture, $O_2^{\bullet -}$ transforms into reactive species like $HO^{\bullet}$, $HO_2^{\bullet}$ and H_2O_2, which act as oxidizing agents. Hole-trapping by the surface hydroxyl groups yields highly active hydroxyl radicals ($OH^{\bullet}$) with high oxidation capability and thus promote the elimination of organic pollutant during the TiO_2 photocatalysis. Moreover, during the process of photocatalytic reaction, oxygen vacancies and defects can become centers to capture photo-induced electrons, so that the recombination of photo-induced electrons and holes can be effectively inhibited. Actually, oxygen vacancies can promote the adsorption of O_2. The adsorbed O_2 may accept e^- and form $O_2^{\bullet -}$ radical groups, which leads to the formation of $^{\bullet}OH$ in the system. The hydroxyl radical groups are active to promote the oxidation of organic substances. Thus, it can be suggested that oxygen vacancies and defects are in favor of photocatalytic reactions in some degree. Therefore, the high density of surface hydroxyl groups on the Au modified TiO_2 nanoparticles may responsible for the enhanced high photocatalytic activity of TiO_2.

In a photocatalytic process, the separation and recombination of photoinduced electron and hole are competitive pathways, and photocatalytic activity is effective when the recombination is prevented. The extent of recombination can be probed by the intensity of photoluminescence. According to the attributes and formation mechanism of PL, there are two types of PL phenomenon: the band–band PL and the excitonic PL [24]. As is displayed in Fig. 6, a strong UV emission emerges at 390 nm with the energy of light approximately equal to the band gap energy of anatase (387.5 nm). Besides, several relatively weak visible emissions in the range of 410–520 nm are observed for both of the oxides. The UV emission is attributed to free excitonic emission near band edge. The visible emissions are due to transition in various kinds of defect states and the subsequent recombination of electrons in singly occupied oxygen vacancy with the photogenerated holes in the VB. Compared with the pure TiO_2, loading Au on TiO_2 leads to a decrease of both the UV and visible emissions. The main reasons responsible for suppression of near band and visible emissions can be ascribed as below. The visible emission (VE) is associated with the structural defects. The decrease of VE implies that the surface defects are eased out partly on depositing pre-sulphated titania matrix with Au combined with the heat-treatment at 600 °C. The decrease of the UV emission for the Au–TiO_2 photocatalyst can be ascribed to the electron trapping effect of Au, which acts as electron acceptor, thus hindering the recombination of charge carriers on TiO_2.

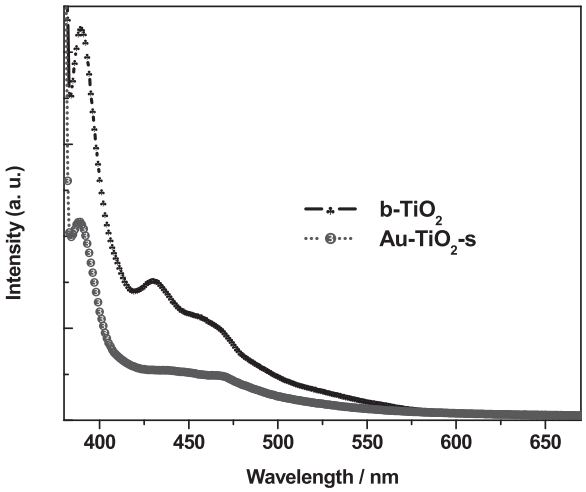

Fig. 6. The room temperature photoluminescence spectra with excitation at 320 nm for the as-prepared photocatalysts.

It is known that the intensity of the emission from the TiO_2 particles is strongly dependent on the surface treatment of the TiO_2 particles. Therefore, the electron trapping effect of Au is favorable for the improvement of the photocatalytic activity of TiO_2 due to the enhancement of the separation efficiency of photogenerated electrons and holes, which can reduce the possibility of excitons quenching and improve the quantum efficiency of photocatalytic reaction. Therefore, the recombination rate of photogenerated electrons and hole was retarded, leading to the reduction of PL signal intensity and this slower recombination process of photogenerated charges will benefit the photocatalytic degradation reaction greatly.

The used dye 'Congo Red (CR)' is in the list of prohibited dye list (Consumer goods which contain aromatic amines originating from azo dyes are prohibited from manufacture and sale in European Union countries since September 2003 because of its toxicity. Congo Red (CR) is a brownish red powder having an absorbance maximum between 497.0 and 500.0 nm in aqueous medium. It is a water soluble secondary diazo dye and contains an azo (—N = N—) chromophore and an acidic auxochrome (sulfonate: $-SO_3H$) associated with the benzene structure. The photocatalytic performances of the different catalysts were investigated by decomposing CR dye under simulated solar light irradiation ($\lambda > 390$ nm). Two steps are involved in the photocatalytic decomposition of aromatic dye, the adsorption of dye molecules, and their degradation. As a precondition for photocatalytic performance, the adsorptivity of CR dye on catalyst was studied after adsorption/desorption equilibrium in the dark. It is found that after adsorption in the dark for 60 min, all the samples reached adsorption-desorption equilibrium. Moreover, the experimental results indicate that the substrate adsorbed by a photocatalyst obeying a Langmuir isotherm and the adsorption equilibrium is maintained during the photocatalytic reaction. Therefore, the slight difference of the initial equilibrium adsorptions is believed not to affect the subsequent comparative discussion on the discrepancy of intrinsic photocatalytic efficiencies of the different materials, and the surface reaction will be viewed as the rate-determining step in photocatalytic reaction as we take the adsorption–desorption equilibrium state as a reference point. Besides, it was found that in the absence of any photocatalyst, the photodecomposition of CR dye under simulated solar light illumination is negligible, which confirms that the decomposition of CR is mainly caused by photocatalytic degradation rather than self-photodecomposition of dye. Therefore, CR was employed as a photocatalysis probe but visible light absorbing dyes like rhodamine B can also mineralize through charge transfer from the dye to the semiconductor (akin to a Dye Sensitized Solar Cell). When using dyes to prove photocatalytic activities, it is necessary to decouple the above parameters either by creating an action spectrum or by running other photocatalytic probes.The influence of solution pH on the removal efficiency of CR dye is investigated tentatively. The results obtained in the pH range 3–9 shows that the enhanced photodegradation was obtained at pH 6.5 for both the catalysts. CR dye can be used as an indicator since it turns from red–brown (in basic medium) to blue in acid medium, and the color of aqueous CR depends upon the concentration of H^+ and OH^- ions. The concentration of the ionized indicator [CR^-] and protonated indicator [HCR] in acidic solutions, and the concentration of hydroxylated indicator [CR—OH] and ionized indicator molecule [CR^+] in alkaline solutions determine the adsorption characteristics. In the presence of excess [H^+] ions in the solution, the ionization will be depressed due to the common ion effect and the concentration [CR^-] will be very small and the color will therefore be that of unionized form. In the alkaline medium the decrease of [H^+] will result in the further ionization of the indicator thereby increasing the color of the ionized form. The concentration of the ionized and unionized forms is thus directly related to the hydrogen ion concentration. The ratios of [CR^-]/[HCR] and [CR—OH]/[CR^+] in acidic and basic solutions determines the adsorption characteristics on the surface of photocatalysts. The point of zero charge (pzc) of the photocatalyst also varies with pH. Below the isoelectric point the surface is positively charged and vice versa. The combined effect of surface charges and ionized concentration of dye molecules will determine the extent of adsorption. Maximum adsorption was observed at pH 6.5 for both the photocatalysts. But the extent of degradation was higher with Au–TiO_2-s in the specified time interval. Due to the multiple roles that various factors could play, such as electrostatic interactions with the semiconductor surface, chemical structure of the target molecule and of its fragments or intermediate formation of active radicals, etc., will dictate the reaction process. Further the capacity of adsorption on bare titania and Au-modified titania at different pH values can be explained by the intrinsic amphoteric behavior (Ti—OH) of suspended catalyst particles and the acidic/basic nature of the dye molecule. The metal oxide photocatalyst particles in aqueous system behave as diprotic acids due to the surface hydroxylation. This photocatalyst surface have active role in the photodegradation reaction. In acidic solution, the possible reactions are: $TiOH + H^+ \rightarrow TiOH_2^+$ ($pH < 6.25$), $TiOH \rightarrow TiO^- + H^+$ ($pH > 6.25$). Due to the higher extent of hydroxylation on Au–TiO_2 (as supported by the FTIR spectroscopic studies) the extent of adsorption of reactive dye molecules seems to be higher [25]. The higher efficiency of metallized Au–TiO_2 can be attributed to (A) high electron affinity by deposited metal and hence increase of lifetime of charge carriers thereby decreasing the rate of recombination, (B) increase in the absorbed light fraction due to the shift in the absorption spectrum of semiconductor to the longer wavelength and (C) accumulation of the holes in the semiconductor particles increases the probability of formation of excited oxygen atom which are reactive species and readily oxidizes the organic dye molecule.

The various possible reactions at Au-TiO_2 surface is as follows: e^- (trapped at Au deposit) + $O_2 \rightarrow O_2^{\bullet -}$, $O_2^{\bullet -} + H^+ \rightarrow HO_2^{\bullet}$. The excess electrons at the Au deposits can further modify $O_2^{\bullet -}$: e^- (trapped at Au deposit) + $O_2^{\bullet -} \rightarrow O_2^{2-}$. This adsorbed peroxide ion can dissociate to O^-, and this further reacts with hole producing an excited oxygen atom: $O_2^{2-} \rightarrow 2O^-$ (absorbed), $O^- + h^+ \rightarrow O^*$. The decrease of pH in the course of the degradation reaction can be accounted to the continuous decomposition of CR and the formation of simple ions like NO_3^-, SO_4^{2-}, CO_2 and H_2O. Effects of pH on the degradation of MO dye indicated that the photocatalytic degradation of CR over Au–TiO_2 was significantly affected by the solution

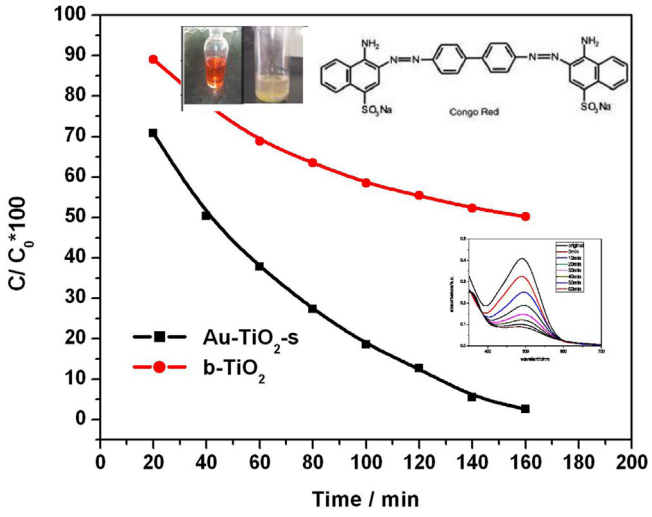

Fig. 7. Decolorization effect on CR dye of bare TiO_2 and Au–TiO_2-s catalysts.

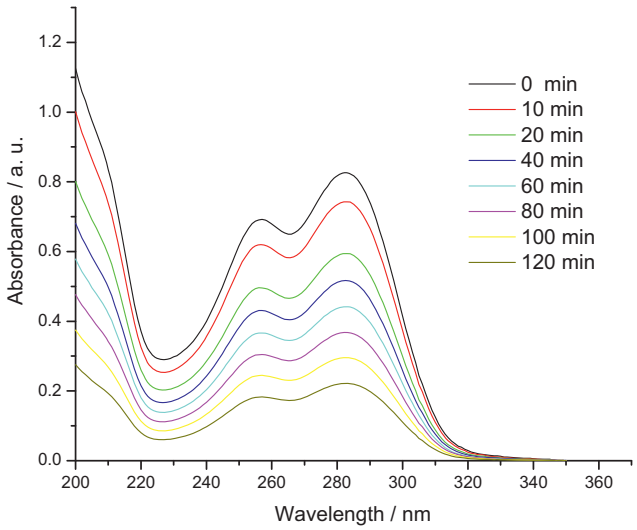

Fig. 8. Degradation effect on pharmaceutical phthalylsulfathiazole (200 mg/L) upon as-prepared Au–TiO_2-s catalyst.

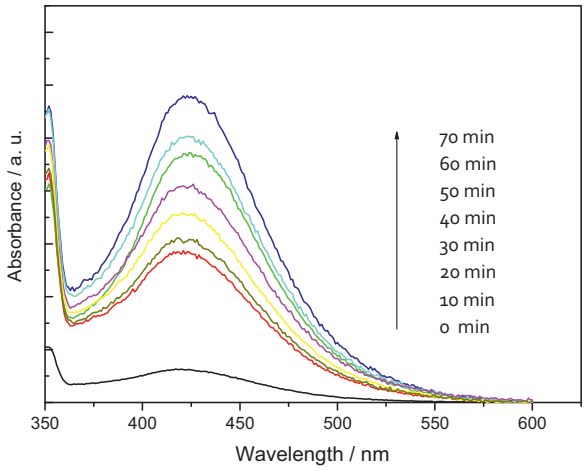

Fig. 9. Photoluminescence spectral changes of terephthalic acid solution in presence of Au–TiO_2-s photocatalyst under excite light irradiation.

pH. The degradation rate of CR decreased drastically with increase or decrease of pH. 89% and 67% of the removal rate of CR were accomplished at pH of 6.5 using Au–TiO_2 and bare TiO_2, respectively, after 120 min of simulated light irradiation. Nonetheless, only 51% and 62% of CR can be degraded at pH 3.0 and 9.0, respectively using Au–TiO_2 catalyst. When pH was higher than 6.5, the surface potential of Au–TiO_2 particle was negative. In an aqueous medium, CR molecule ionizes as CR anion and two sodium cations. The electrostatic repulsion between CR anion and photocatalyst particle increased and the adsorbed amount of CR decreased with increase of pH, resulting in decrease in degradation rate for CR. Other studies indicate that the positions of both valence and conduction band depend on the pH of the solution and the potential of these bands shifts by about 59 mV more toward the negative potential as the pH increases by one unit at 25 °C [26]. Photocatalytic activity of the sulfated Au–TiO_2 and unmodified TiO_2 samples, was evaluated following the reaction of CR photo-oxidation at optimum conditions (pH level was adjusted to be 6.5). Photochemical breakdown of the chromophoric groups (—N = N—) present in the CR molecule is monitored by UV–vis spectrophotometer and CR concentration was measured by UV–vis spectrometry following its 498 nm characteristic band attributed to azo form. Fig. 7 represents the photodegradation of CR dye as a function of irradiation time over different photocatalysts. As is shown, after irradiation for 120 min, the photodegradation efficiency of CR dye on bare TiO_2 was 55.0%. But for the Au modified titania photocatalyst, the photodegradation efficiency could reach 90% when subjected to illumination for 120 min. The complete mineralization of the dye has to be verified by recording the absorption spectrum for the solution containing the dye after irradiation, as shown in inset of Fig. 7.

The obtained result suggests that surface modification of TiO_2 with Au nanoparticles improves the photocatalytic activity under simulated solar light, which may be attributed to not only increase in visible light absorption, but also enhancement of charge separation (e^-/h^+) by trapping photoelectrons on gold nanoparticles. Gold modified titania system has a better degradation effect than bare TiO_2 because metal nanoparticles deposited to TiO_2 nanostructures undergo Fermi level equilibration and enhance the charge-transfer process [27]. As known, the photocatalytic reaction takes place on the surface of the catalysts and recombination of photogenerated electrons and holes is very fast. The enhanced photoreactivity can be explained by the transfer of photogenerated electrons from TiO_2 to the metal particles, inhibiting electron-hole recombination and thus raising the oxidation efficiency of the positive holes generated in the valence band of TiO_2. Metal nanoparticles can act as electron traps due to the fact that when a metal and a semiconductor of different Fermi level position come into contact, electrons flow to the metal from the semiconductor to align Fermi level, resulting in surface charge layer at interface. The electrical barrier originated from surface charge layer at metal-semiconductor interface is called Schottky barrier [28]. Contact between Au and a TiO_2 surface can naturally lead to the formation of a Schottky barrier, resulting in the transfer of photogenerated electrons into Au, which acts as electron trapping islands inhibiting e^-/h^+ recombination [29–31]. To investigate the mechanism of the photocatalytic activity Au/TiO_2/S, the •OH which formed on a photo-illuminated different catalysts surface was detected by a photoluminescence (PL) method using terephthalic acid as a probe molecule, the results are shown in (Fig. 9). The fluorescence intensity was proportional to the amount of •OH produced. It was observed that Au/TiO_2/S can produce •OH after xenon lamp irradiation. And the fluorescence intensity of Au/TiO_2/S at 425 nm increases along with irradiation time. Generally, two competitive processes, charge carriers recombination versus interfacial charge transfer, may occur after the creation of photo-generated charge carriers. The former eliminated the photo-generated electrons and holes, while the latter produced

active radical species (e.g., •OH, O_2^-, H_2O_2). A small quantity of loaded metallic Au prevents the direct recombination of electrons and holes. And then low recombination rate of electrons and holes is result in high photocatalytic activity. The presence of pharmaceuticals in the environment is a growing concern. It is well known that pharmaceutical phthalylsulfathiazole is among the most widely used antimicrobials in human and veterinary medicine. This kind of antimicrobials shows high resistance to biological degradation, and has been detected in wastewater, surface water, and groundwater samples. As shown in Fig. 8, the as-prepared catalyst also shows the good photocatalytic ability upon decomposition of pharmaceutical phthalylsulfathiazole.

Actually, the oxidation by the photogenerated holes and oxidizing radicals at the semiconductor/metal interface is an important process. It can be a major factor in determining the overall photocatalytic efficiency of metal-semiconductor nanocomposites. After excitation the electron migrates to the metal where it becomes trapped and the hole-electron recombination is suppressed. The hole is then free to diffuse to the semiconductor surface where oxidation of organic substances can occur. Gold particles deposited on the surface of titania can act as electron-hole separation center. Because the Fermi level of gold is lower than that of TiO_2 the movement of photogenerated electrons from the CB of TiO_2, leaving behind the holes in the VB, to the gold particles deposited on the surface of TiO_2 is thermodynamically feasible. Therefore, the photoinduced electrons transfer to the interfacial surface of excited TiO_2 and then to the Au nanoparticles until the Fermi level equilibrium will be attained. This migration of the generated electrons to metal particles can retard the fast e^-/h^+ recombination and increase the lifetime of the holes. Some of electrons can be transferred to the TiO_2 surface and reduce the dissolved O_2 easily, because dissolved oxygen is also one of the good accepters of electrons. The photo-generated holes on the TiO_2 surface can react with water to produce powerful oxidative radicals OH•and HO_2 •. The Au nanoparticles act as a schottky barrier of TiO_2 to capture transferred electrons because of its strong electron-accepting ability and resulting in the effective separation e^-/h^+ pairs as confirmed by the PL measurements. Accordingly, more electrons and holes can be produced, leading to enhanced quantum efficiency of photocatalysis. As a result the photoinduced solid-liquid interfacial charge-transfer processes are promoted and the photocatalytic dye decomposition than TiO_2 alone is enhanced. Therefore, the enhancement in the photocatalytic activity of TiO_2 by the surface deposition of gold nanoparticles can be ascribed to an improvement of charge separation. The metal particles act as sinks for the photogenerated electrons, which reduces charge recombination and consequently increases the efficiency of the photocatalytic process. The metal is also important for the photocatalytic properties of the semiconductor by changing the distribution of electrons. For example, the metal and the n-type semiconductor such as titania have different Fermi level positions. The metal has a higher work function than the semiconductor. When the two species come in contact with the Fermi levels of the metal and the semiconductor, electrons are caused to flow to the metal from the semiconductor. The decrease in electron density within the semiconductor leads to an increase in the hydroxyl group acidity, as confirmed by the FT-IR measurements. This in turn affects the photocatalytic process on the semiconductor surface, where Au islands are adhered in selected locations on TiO_2 nano-clusters and redox reactions can be further sustained if reduction of oxygen resulting in the generation of superoxide anions is galvanically promoted on the Au nanoparticles. Moreover, the tail of the localized surface plasmon resonance in the near-UV region can have an effect on the photocatalytic activity [32–34]. Surface plasmon resonance absorption is associated with a significant enhancement of the electric near field in the vicinity of the Au nanoparticles. It was reported that the enhanced near-field could boost the excitation of electron-hole pairs in TiO_2 or other semiconductors and therefore sustaining the photochemical reaction [35–49]. At last, the influence of the gold deposition procedure on the structural and photocatalytic properties should be considered, and this is another factor affecting the photocatalytic efficiency of the Au–TiO_2 composite.

3. Conclusions

The deposition of nanosized gold particles on the titania surface increases the photocatalytic activity of the semiconductor oxide, by increasing the efficiency of charge separation of the photogenerated electron-hole pairs. The presence of gold mainly enhances the photocatalytic oxidation of organic compounds that are predominately oxidized by holes. The enhancement is due to the electron attracting and trapping by the metal deposit, higher extent of light absorption and degree of hydroxylated surface will dictate the photocatalytic reaction in Au deposited catalyst. Further, accumulation of the holes in the semiconductor particles increases the probability of formation of excited oxygen atom which is a reactive species and readily oxidizes the CR dye molecule. The degradation is most efficient at pH 6.5 for both the catalysts which depends on the concentration of the various ions formed and also on the nature of the catalyst. But the extent of degradation was higher with Au–TiO_2 in the specified time interval. This is due to the higher extent of surface hydroxylation on Au–TiO_2 leading to the higher extent of adsorption of reactive dye molecules. The combined effect of surface charges and ionized concentration of dye molecules will determine the extent of adsorption. It was found that under optimal experimental conditions the percentage of dye removal is found to be 97.6% at pH 6.5 during 160 min reaction period.

Acknowledgments

This work was supported by Natural Science Foundation of Hubei Province of China (project no. 2011CDB148) and the Fundamental Research Funds for the Central Universities(program no. 2013QC026).

References

[1] M.A. Brown, S.C. Devito, Crit. Rev. Environ. Sci. Technol. 23 (1993) 249.
[2] S. Sajjad, S.A.K. Leghari, J.L. Zhang, RSC Adv 3 (2013) 12678.
[3] S.W. Zhang, J.X. Li, H.H. Niu, W.Q. Xu, J.Z. Xu, W.P. Hu, X.K. Wang, ChemPlusChem 78 (2013) 192.
[4] J.L. Zhang, Y.M. Wu, M.Y. Xing, S.A.K. Leghari, S. Sajjad, Energy Environ. Sci. 3 (2010) 715.
[5] S.W. Zhang, J.X. Li, M.Y. Zeng, G.X. Zhao, J.Z. Xu, W.P. Hu, X.K. Wang, ACS Appl. Mater. Interfaces 5 (2013) 12735.
[6] G.G. Zhang, M.W. Zhang, X.X. Ye, X.Q. Qiu, S. Lin, X.C. Wang, Adv. Mater. 26 (2014) 805.
[7] X.D. Zhang, X. Xie, H. Wang, J.J. Zhang, B. Pan, Y. Xie, J. Am. Chem. Soc. 135 (2013) 18.
[8] Y.J. Zhang, M. Antonietti, Chem. Asian J. 5 (2010) 1307.
[9] J.S. Zhang, J.H. Sun, K. Maeda, K. Domen, P. Liu, M. Antonietti, X.Z. Fu, X.C. Wang, Energy Environ. Sci. 4 (2011) 675.
[10] J. Zhang, F.J. Shi, J. Lin, D.F. Chen, J.M. Gao, Z.X. Huang, X.X. Ding, C.C. Tang, Chem. Mater. 20 (2008) 2937.
[11] S. Sajjad, S.A.K. Leghari, J.L. Zhang, RSC Adv. 3 (2013) 1363.
[12] J. Zhang, C.X. Pan, P.F. Fang, J.H. Wei, R. Xiong, ACS Appl. Mater. Interfaces 2 (2010) 1173.
[13] S.W. Zhang, J.X. Li, M.Y. Zeng, J. Li, J.Z. Xu, X.K. Wang, Chem. Eur. J. 20 (2014) 9805.
[14] H.J. Zhang, G.H. Chen, D.W. Bahnemann, J. Mater. Chem. 19 (2009) 5089.
[15] K.Z. Zhang, B.Z. Lin, Y.L. Chen, B.H. Xu, X.T. Pian, J.D. Kuang, B. Li, J. Colloid Interf. Sci. 358 (2011) 360.
[16] S.A.K. Leghari, S. Sajjad, J.L. Zhang, RSC Adv. 3 (2013) 15354.
[17] D.F. Zhang, Russ. J. Phys. Chem. A 88 (2014) 2252.
[18] D.F. Zhang, Russ. J. Phys. Chem. A 88 (2014) 2476.
[19] Z. Zhang, S. Ito, J.E. Moser, S.M. Zakeeruddin, M. Gratzel, ChemPhysChem 10 (2009) 1834.
[20] S.A.K. Leghari, S. Sajjad, J.L. Zhang, RSC Adv. 4 (2014) 5248.
[21] L. Zhang, J.C. Yu, Catal. Commun. 6 (2005) 684.

[22] F. Zhang, Y. Pi, J. Cui, Y. Yang, X. Zhang, N. Guan, J. Phys. Chem. C 111 (2007) 3756.
[23] J.T. Zhang, Z.G. Xiong, X.S. Zhao, J. Mater. Chem. 21 (2011) 3634.
[24] J. Zhang, Q.L. Xu, S.Z. Qiao, J.G. Yu, ChemSusChem 6 (2013) 2009.
[25] M.Y. Xing, W.Z. Fang, X.L. Yang, B.Z. Tian, J. Zhang, Chem. Commun. 50 (2014) 6637.
[26] J. Zhang, S.Z. Qiao, L.F. Qi, J.G. Yu, Phys. Chem. Chem. Phys. 15 (2013) 12088.
[27] X.F. Yan, L.Z. Wang, D.Y. Qi, J.Y. Lei, B. Shen, T. Sen, J.L. Zhang, RSC Adv. 4 (2014) 57743.
[28] F.J. Zhang, J. Liu, M.L. Chen, W.C. Oh, J. Korean Ceram. Soc. 46 (2009) 263.
[29] J. Li, Y. Yu, L.Z. Zhang, Nanoscale 6 (2014) 8473.
[30] J. Zhang, J.G. Yu, M. Jaroniec, J. Ru Gong, Nano Lett. 12 (2012) 4584.
[31] J. Zhang, L. Xiao, Y. Cong, M. Anpo, Top. Catal. 47 (2008) 122.
[32] J. Zhang, J.G. Yu, Y.M. Zhang, Q. Li, J.R. Gong, Nano Lett. 11 (2011) 4774.
[33] G.H. Dong, Z.H. Ai, L.Z. Zhang, RSC Adv. 4 (2014) 5553.
[34] J. Zhang, S.W. Liu, J.G. Yu, M. Jaroniec, J. Mater. Chem. 21 (2011) 14655.
[36] J. Jiang, L.Z. Zhang, H. Li, W.W. He, J.J. Yin, Nanoscale. 5 (2013) 10573.
[37] H. Li, L.Z. Zhang, Nanoscale 6 (2014) 7805.
[38] G.H. Dong, K. Zhao, L.Z. Zhang, Chem. Commun. 48 (2012) 6178.
[39] J. Li, L.Z. Zhang, Y.J. Li, Y. Yu, Nanoscale 6 (2014) 167.
[40] R.F. Dong, B.Z. Tian, C.Y. Zeng, T.Y. Li, T.T. Wang, J.L. Zhang, J. Phys. Chem. C 117 (2013) 213.
[41] D.Y. Qi, M.Y. Xing, J.L. Zhang, J. Phys. Chem. C 118 (2014) 7329.
[42] T.Y. Li, B.Z. Tian, J.L. Zhang, R.F. Dong, T.T. Wang, F. Yang, Ind. Eng. Chem. Res. 52 (2013) 6704.
[43] B.C. Qiu, M.Y. Xing, J.L. Zhang, J. Am. Chem. Soc. 136 (2014) 5852.
[44] D.Y. Qi, L.J. Lu, L.Z. Wang, J.L. Zhang, J. Am. Chem. Soc. 136 (2014) 9886.
[45] K. Su, Z.H. Ai, L.Z. Zhang, J. Phys. Chem. C 116 (2012) 17118.
[46] X. Ding, K. Zhao, L.Z. Zhang, Environ. Sci. Technol. 48 (2014) 5823.
[47] J. Jiang, K. Zhao, X.Y. Xiao, L.Z. Zhang, J. Am. Chem. Soc. 134 (2012) 4473.
[48] K. Zhao, L.Z. Zhang, J.J. Wang, Q.X. Li, W.W. He, J.J. Yin, J. Am. Chem. Soc. 135 (2013) 15750.
[49] G.H. Dong, L.Z. Zhang, J. Phys. Chem. C 117 (2013) 4062.